Available online at www.sciencedirect.com

ScienceDirect

Ceramics International 40 (2014) 3193–3198

CERAMICS INTERNATIONAL

www.elsevier.com/locate/ceramint

Synthesis of ZnO/Cu micro and nanostructures via a vapor phase transport method using different tube systems

A. Kamalianfar[a,b,**], S.A. Halim[a,*], A. Khorsand Zak[c]

[a]Department of Physics, Faculty of Science, University Putra Malaysia, UPM, 43400 Serdang, Selangor, Malaysia
[b]Department of Physics, Farhangian University, Iran
[c]Nanotechnology Laboratory, Esfarayen University, Esfarayen, North Khorasan, Iran

Received 4 September 2013; received in revised form 25 September 2013; accepted 27 September 2013
Available online 8 October 2013

Abstract

ZnO micro and nanostructures were grown on copper coated silicon substrates using two different systems: an opened system (both ends opened tube) and a closed system (one closed end tube). The thermodynamic conditions of the systems made a significant difference in boundary layer and super-saturation between the systems. The results indicate that diffusion of the gaseous species through the boundary layers at low and high pressures controls the final formation of the morphologies. The ZnO nanostructures which have been grown in a restricted place have larger diameters and lengths. The structure of the products was analyzed by X-ray diffractometer (XRD) and it was found that the good crystalline quality of the samples was obtained in a closed system. To study the optical properties, photoluminescence (PL) and ultra violet–visible (UV–vis) spectroscopy were employed. It was observed that a decrease in the growth temperature of the opened system caused a broad and dominant visible emission covering the blue and green emission in the PL spectra.
© 2013 Elsevier Ltd and Techna Group S.r.l. All rights reserved.

Keywords: D. ZnO; Nanostructure; Hierarchical; Thin film; Vapor method

1. Introduction

Hierarchical structures are new class of materials formed by combination of two types of semiconductors or metal oxides such as ZnO, TiO2, ZnS, CdS, CuO and so on. The coupling between two different semiconductor oxides can improve the optical properties by shifting absorption edge toward the higher wavelength and changing the band gap [1,2]. Zinc oxide is a widely studied n-type semiconductor, with wide direct band gap (Eg=3.37 eV) and high value exciton binding energy (~60 meV) and has been used in optoelectronic devices, UV detection lasers, and sensors [3,4]. On the other side, copper oxide is a metal oxide with a narrow direct band gap of 1.2 eV, p-type semiconductivity and sensing properties. Thus, the chemical compatibility of ZnO with other oxide materials such as CuO provides a p–n semiconductor heterojunction, making it a promising candidate for applications in humidity and gas sensors [5,6]. Various methods have been used to fabricate ZnO nanostructures including PLD [7], physical vapor deposition (PVD) [8], chemical vapor deposition or vapor phase transport (CVD, VPT) [2,9,10], solvo- and hydro-thermal [11,12], sol–gel [13,14], combustion [15], and sonochemical [16]. Among of these methods, VPT is the common method that has been used to prepare high purity of ZnO nanostructures [17,18]. In this method the morphology of micro and nanostructures depends on the growing conditions including the position of substrates, source materials, gas flow rates, substrate temperatures and difference in vapor super-saturation. Depending on the different vapor super-saturation and distance between sources to substrate, various kinds of morphologies, such as wires, rods, disks and flowers could be obtained. A variation in the gas flow rate affects the qualitative super-saturation profile and consequently the structural, electrical and optical properties of ZnO micro and nanostructures.

In this work, we study the effect of boundary layer thickness on the morphological and optical properties of ZnO micro and nanostructures grown on copper coated silicon substrates using a vapor phase transport (VPT) method. Two types of quartz

*Corresponding author at: Department of Physics, Faculty of Science, University Putra Malaysia, 43400 UPM Serdang, Selangor, Malaysia. Tel.: +60 11 1541 7865.
**Corresponding author.
E-mail address: kamalianfar.ahmad@gmail.com (A. Kamalianfar).

0272-8842/$ - see front matter © 2013 Elsevier Ltd and Techna Group S.r.l. All rights reserved.
http://dx.doi.org/10.1016/j.ceramint.2013.09.123

tube were used to apply different thermodynamic conditions on the samples. The relation between optical properties, morphologies, and thermodynamic condition is discussed in details. Finally, the effect of vapor super-saturation on the optical properties of the samples is investigated.

2. Materials and methods

2.1. Experimental

Silicon (111) was used as substrate and first ultrasonically cleaned in acetone and ethanol for 30 min. A thin layer of copper with 50 nm thickness was deposited on the substrates by the sputtering technique (Kurt J. Lesker 75). The setup included a both ends opened (B.E.O) quartz tube and one closed end (O.C.E) quartz tube. A mixture of zinc oxide (99.99%) and commercial graphite powder (1:1 weight rate) was loaded onto the alumina boats which were transferred to the quartz tubes at the central of an electrical furnace tube (100 cm length and 5 cm diameter) as shown in Fig. 1.

The copper coated silicon substrates were adjusted in near, middle and far from the source in the quartz tubes. Based on the furnace temperature calibration, the temperatures of the substrates were fixed at 800, 650 and 500 °C, respectively. The furnace was heated up to 900 °C with heating rate of 20 °C/min. Pure nitrogen gas was fed into the furnace tube at a constant flow rate of 70 sccm (standard cubic centimeters per minute) When the temperature of the furnace reached at 800 °C. The temperature of the source (900 °C) and gas flow rate were kept constant during the growing process for 1 h. Finally, the electric furnace was naturally cooled down to the room temperature.

The products were characterized by a field emission scanning electron microscopy (FESEM, JSM 6700) and X-ray diffractometer (XRD, Shimadzu 6000) employing CuKα (0.154 nm) radiation. The PL measurements were performed at room temperature by a fluorescence spectrometer (LS 55, Xe lamp). Absorption plots of the samples were obtained using ultraviolet–visible spectroscopy (UV–vis 3600 SHIMADZU).

2.2. Theory of the growth mechanism in different conditions

In the O.C.E system, diffusion of the gaseous species from regions of higher concentration to regions of lower concentration inside the quartz tube causes gaseous species to flow downstream. In this system, diffusion can still occur when there is no concentration gradient but there is a spatial difference in the chemical potential. In the B.E.O system, the gaseous species are transferred from the source region to the substrate with the assistance of gas flow across the temperature gradient.

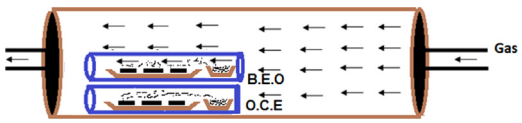

Fig. 1. Schematically illustration of the O.C.E and B.E.O systems.

One-dimensional diffusion of a gas described by Fick's first law:

$$J = -D\frac{dc(x)}{d(x)}$$

Where J is the diffusion flux (amount of substance per unit area per unit time), D is the intrinsic diffusion coefficient and c is concentration at x.

In both systems, the gaseous species transport from the source region to the substrates through a layer of reduced velocity vapor, called boundary layer, as shown in Fig. 2. The gas flowing in the B.O.E tube must diffuse through the boundary layer to reach to the surface of substrate. The main difference between the thickness of the boundary layer in the O.C.E and B.O.E tube systems is due to the gas velocity. In the B.O.E tube the thickness of the boundary layer is lower than that of the B.O.E. The thickness of the boundary layer affects the surface reaction, adsorption and determine the overall growth rate obtaining different morphologies. Dependence of the growth rate on substrate orientation is a sign of this claim. When the gaseous species reach the surface, adsorption and chemical reactions occur on it. In this situation, the boundary layer transports the diffused atoms to growth sites providing nucleation and final morphology.

3. Results and discussion

Fig. 3 shows the FESEM images of the as-grown ZnO micro/nanostructures on the copper coated Si (111) substrates using two different tube systems. Fig. 3a and b shows the growth of short, thin and sparse wires on the surfaces grown in both of the tubes at 800 °C, which is the highest substrate temperature and closer to the material source. Fig. 3a exhibits multipods crystal consists of a number of legs unite at the same junction with several micrometer lengths and 100–150 nm diameter. Also, Fig. 3b presents the growth of dense and long nanospears with an average diameter of 100–150 nm. The high temperature and pressure in this area increases the thickness of the boundary layer and limits the gaseous species to diffuse through. Therefore, a high rate of desorption and revaporation due to the high temperature and sufficient energy of the vapors causes a rapid nanowire growth with a minimum nanocrystal diameter.

At low pressures and temperatures, the boundary layer is thin and gaseous species easily diffuse through the boundary layer. In these conditions, surface reactions are the main factor to control the growing rate. Fig. 3c and d shows the obtained morphologies at 650 °C. Bunches of grapes-like ZnO structure were observed on the surface of substrate placed into the B.E.O tube. The grapes ranged from 100 to 500 nm. In opposite, the

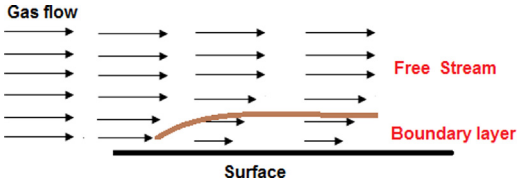

Fig. 2. Illustration of a boundary layer.

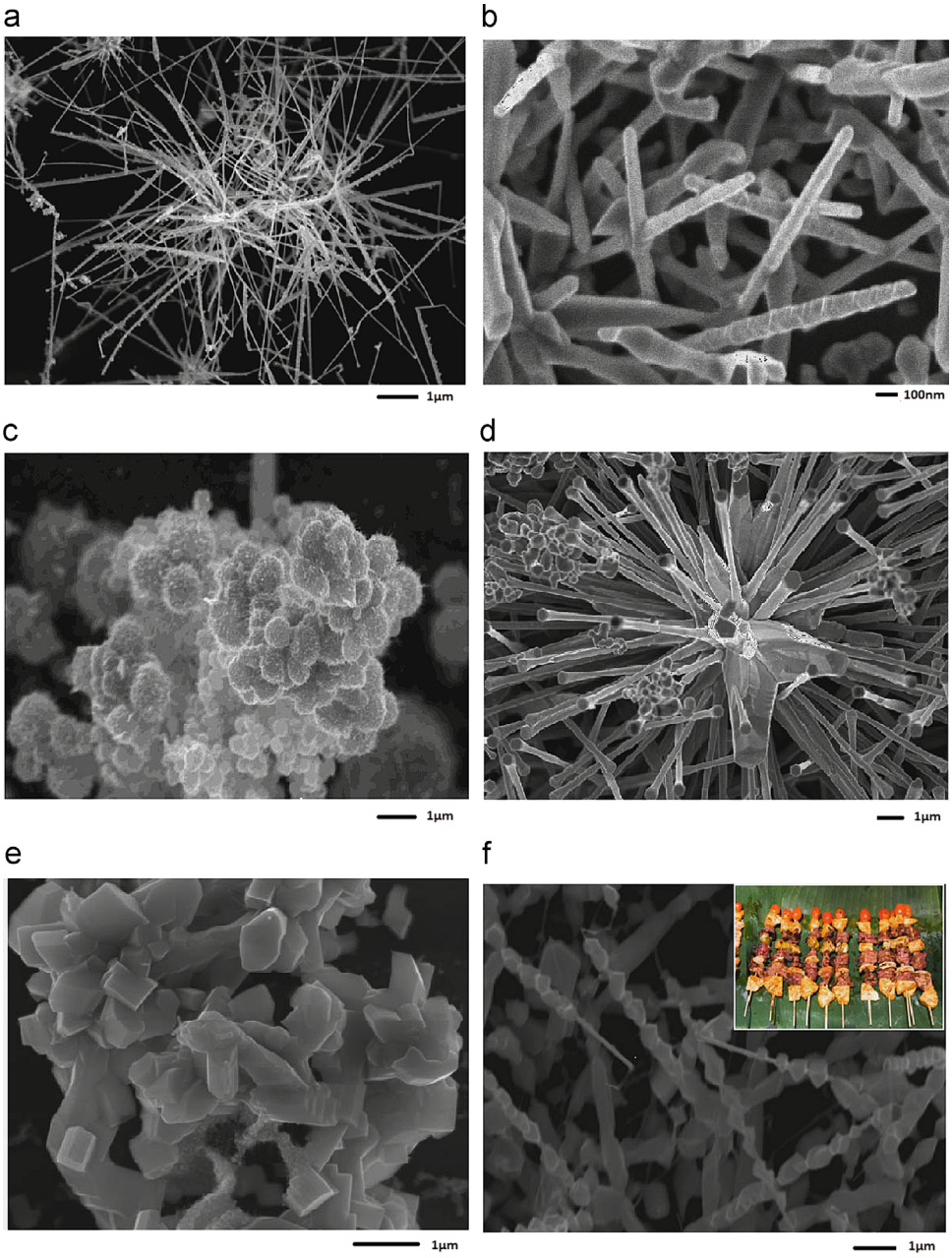

Fig. 3. FESEM images of the as-grown ZnO micro/nanostructures on the copper coated Si (111) substrates using two different system geometries and substrate temperatures. (a), (c) and (e) B.E.O tube and (b), (d) and (f) O.C.E tube.

ZnO club-like ZnO structure was obtained on the surface of the substrate placed into the O.C.E tube at the same temperature (Fig. 3d). The clubs represented a hexagonal cross-section at the end and tended to align quasi-vertically along the normal to the substrate. The length of clubs is several micrometers with average diameter of 400–500 nm.

Fig. 3e shows flower-like ZnO morphology obtained using the B.E.O tube at the lowest temperature zone (550 °C) and formation of barbecue-like ZnO structures at about 550 °C in the O.C.E tube is shown in Fig. 3f. The barbecues composed several pieces with different shapes and sizes. Some nanowires like skewer are present among the pieces. Because this sample was close to the open tube edge and therefore, the collision between ZnO vapors and N_2 affected the flow uniformity of the ZnO vapors in this zone, resulting in formation of ZnO pieces with different shapes and sizes.

The crystal structures of the products were investigated using XRD analysis. Fig. 4 shows the XRD patterns of the samples grown by different system geometries and substrate temperatures. The observed peaks in the patterns can be indexed to a hexagonal wurtzite structure of ZnO (JCPDS No. 800075). The patterns exhibit two main peaks of CuO (111) and Cu (111) (JCPDS No. 0011117 and 0851326). The presence of the copper oxide peak is due to the oxidation of copper at the temperature above 550 °C. For sample (f), the copper oxide peak was not detected. The possibility of the low temperature and inadequate

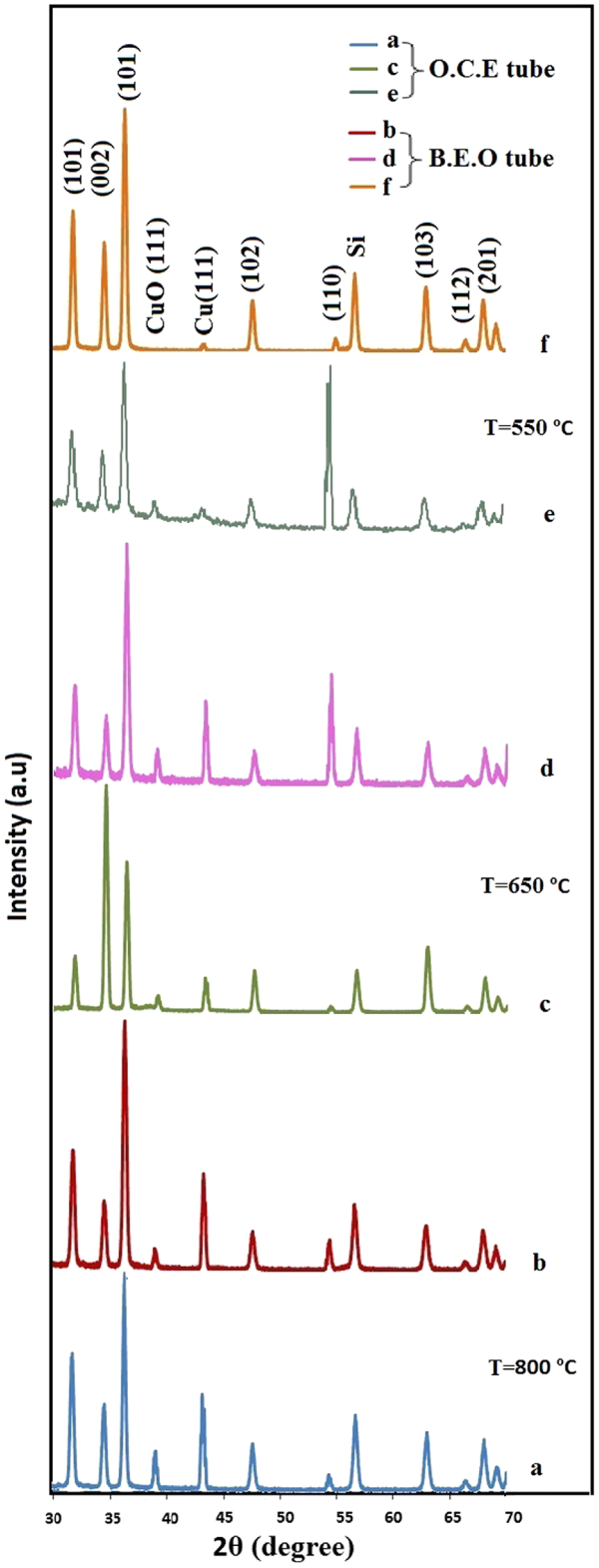

Fig. 4. XRD patterns of the samples grown by different system geometries and substrate temperatures (a), (c) and (e) B.E.O tube and (b), (d) and (f) O.C.E tube.

of oxygen in its region cannot be ruled out. The XRD results also represent that the preferred orientation of sample (d) is (0 0 2). This *c*-axis preferred orientation agrees with the corresponding FESEM image. Some structural parameters of the patterns are listed in Table 1. A comparison between the first two peaks of the ZnO patterns indicates that the full width at half maximum (FWHM) of the samples, which have been grown using the O.C.E tube is smaller than those of the samples grown using the B.E.O tube. This means the samples grown using the O.C.E tube exhibit a better crystallite quality compared to the one grown in B.E.O.

Fig. 5 displays the room temperature PL spectra of the samples. The ultraviolet (UV) emission band is attributed to the near-band edge (NBE) free exciton transition from the localized level below the conduction band to the valance band [19]. Voss et al. [20] reported that different growth conditions change the relative contributions of free exciton emission and phonon. The relative contributions influence the position of the near-and-edge emissions in the range of 373–390 nm.

As mentioned earlier, the boundary layer thickness depends on temperature and pressure. The intensity of the UV peak is found to be increased with the increase in boundary layer thickness , accompanied by narrowing of the peak in both tubes. The improved UV emission of the samples is assigned to their better overall crystallinity. It can be explained as a

Table 1
A comparison between the first two peaks of the ZnO XRD patterns.

Sample	XRD peak	Degree	Temperature (°C)	Type of tube	FWHM
a	(100)	31.85	~800	B.E.O	0.1574
	(200)	34.42	~800	O.C.E	0.1200
b	(100)	31.84	~800	B.E.O	0.1378
	(200)	34.45	~800	O.C.E	0.0984
c	(100)	31.83	~650	B.E.O	0.3542
	(200)	34.44	~650	O.C.E	0.1378
d	(100)	31.84	~650	B.E.O	0.0960
	(200)	34.52	~650	O.C.E	0.3600
e	(100)	31.86	~550	B.E.O	0.3936
	(200)	34.56	~550	O.C.E	0.3149
f	(100)	31.85	~550	B.E.O	0.2755
	(200)	34.47	~550	O.C.E	0.2588

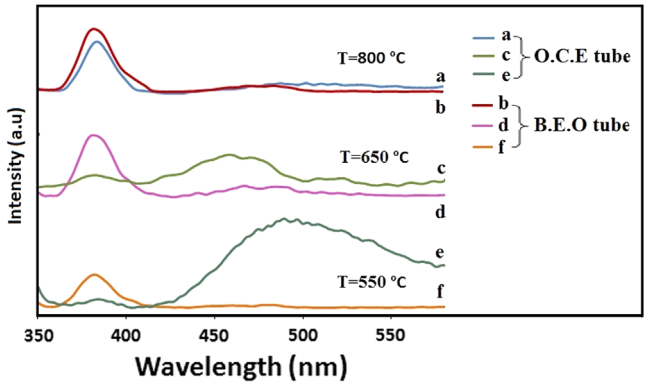

Fig. 5. PL spectra of the as-grown ZnO micro/nanostructures on the copper coated Si (111) substrates using two different system geometries and substrate temperatures. (a), (c) and (e) B.E.O tube and (b), (d) and (f) O.C.E tube.

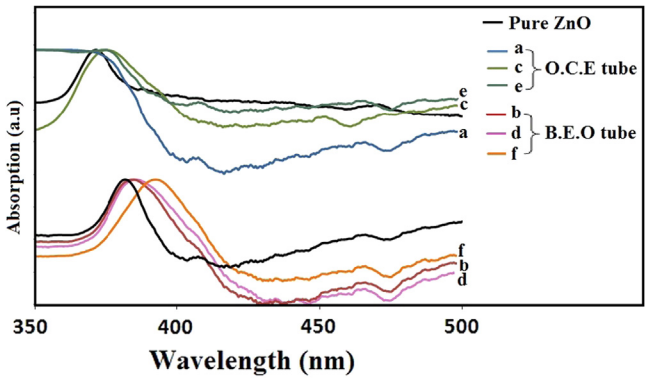

Fig. 6. Absorption spectra of the as-grown ZnO micro/nanostructures on the copper coated Si (111) substrates using two different system geometries and substrate temperatures. (a), (c) and (e) B.E.O tube and (b), (d) and (f) O.C.E tube.

reduction of strain and defects as well as an improvement in crystallite size as supported by the structural investigations.

UV/DLE ratio is one of the main factors that uses for comparing optical properties between samples. The nanostructures grown in the O.C.E tube exhibit a stronger UV peak and a weaker visible emission peak than those in the B.E.O tube. Thus, the UV/DLE ratio of the samples grown in the O.C.E tube is bigger than that in the B.E.O tube. Therefore, the crystalline quality of the products grown in the O.C.E tube is higher than that of in the B.E.O tube.

In the high temperature zone where the boundary layer is thin, the Pl behavior of samples a and b is similar. Comparison between the samples grown at high and low temperatures indicates that the thickness of the boundary layer affected the crystallinity of the samples. The boundary layer transports the diffused atoms to growth sites providing the nucleations and final morphology. At high temperature, the growing rate is very fast, so the gas flow has a lower effect on nucleation and formation of samples.

The visible light spectra region includes one or more emission bands which originate from different deep-level emissions (DLEs). They mainly relate to various defects. A number of hypotheses have been suggested for each defect emission. Thus, difference in the UV emissions can be attributed to the growth conditions and methods. As mentioned before, the visible emission comprised of blue and green bands. The blue emission originates from radiative defects at the interface of ZnO components or interstitial Zn [21]. As a controversial visible emission band in ZnO, green emission has been studied and a variety of hypotheses have been suggested to explain it, including copper impurities [22], Zn vacancies [23] and singly ionized oxygen vacancy [24]. Based on the FESEM images, the dimension of ZnO nanostructures grown using O.C.E tube is larger. In the O.C.E tube, the amount of oxygen is more due to reduction of ZnO, thus the green emission is reduced due to the O_2-rich atmosphere. Thus, the intensity of the green emission in the samples can be attributed to the singly ionized oxygen vacancy (VO) in ZnO nanostructures.

The optical property of ZnO nanostructures was also investigated by UV–visible absorbance spectroscopy. Fig. 6 shows the result of the absorption spectrum for the nanostructures grown in two types of tubes. As a point of reference, the absorption of typical ZnO structures grown on clean silicon substrates at 800 °C using both methods are shown as well. The absorption edges of the pure ZnO samples grown using the B.E.O and O.E.O tubes can be seen at 370 and 380 nm, respectively. The absorption edge shifts to the higher wavelength with increasing the substrate temperature. The red shift may be due to the quantum size effect. Comparison between the pure ZnO and Cu–ZnO nanocomposites indicates that the intensity of the absorption in range of 400–500 nm reduced by introducing copper on the substrate surfaces.

4. Conclusion

Two sets of ZnO nanostructures were grown on copper coated silicon substrates in different tubes using the vapor phase transfer method. The setup included two types of quartz tubes (both ends opened tube and one closed end tube). The boundary layer transports the diffused atoms to the growth sites providing nucleation and final morphology. The results showed that the samples grown in the one closed end tube have bigger diameters and lengths. The pressure and temperature at substrate positions affected the thickness of the boundary layer over the substrates surface and various morphologies of ZnO were obtained. The formation of various morphologies is due to the thermodynamic conditions inside the tubes. The intensity of the UV peak is found to be increased with the boundary layer thickness, accompanied by narrowing of the peak in both tubes. In the O.C.E tube, the green emission of the PL spectra reduced due to the O_2-rich atmosphere.

Acknowledgment

This work was supported by the Universiti Putra Malaysia through Grant nos. ERGS 5527047 and RUGS 9199835 (2011).

References

[1] C. Xu, L. Cao, G. Su, W. Liu, H. Liu, Y. Yu, X. Qu, Preparation of ZnO/Cu2O compound photocatalyst and application in treating organic dyes, Journal of Hazardous Materials 176 (1) (2010) 807–813.

[2] R. Yousefi, A. Zak, Growth and characterization of ZnO nanowires grown on the Si (111) and Si (100) substrates: optical properties and biaxial stress of nanowires, Materials Science in Semiconductor Processing 14 (2) (2011) 170–174.

[3] M.H. Huang, S. Mao, H. Feick, H. Yan, Y. Wu, H. Kind, E. Weber, R. Russo, P. Yang, Room-temperature ultraviolet nanowire nanolasers, Science 292 (5523) (2001) 1897–1899.

[4] Q. Wan, Q. Li, Y. Chen, T. Wang, X. He, J. Li, C. Lin, Fabrication and ethanol sensing characteristics of ZnO nanowire gas sensors, Applied Physics Letters 84 (18) (2004) 3654–3656.

[5] Y. Hu, X. Zhou, Q. Han, Q. Cao, Y. Huang, Sensing properties of CuO–ZnO heterojunction gas sensors, Materials Science and Engineering: B 99 (1) (2003) 41–43.

[6] A. Zainelabdin, G. Amin, S. Zaman, O. Nur, J. Lu, L. Hultman, M. Willander, CuO/ZnO Nanocorals synthesis via hydrothermal technique: growth mechanism and their application as Humidity Sensor, Journal of Materials Chemistry 22 (23) (2012) 11583–11590.

[7] A. Kamalianfar, S. Halim, K. Behzad, M.G. Naseri, M. Navasery, F.U. Din, J. Zahedi, K. Lim, S. Chen, H. Sidek, Effect of thickness on structural, optical and magnetic properties of Co doped ZnO thin film by

pulsed laser deposition, Journal of Optoelectronics and Advanced Materials 15 (3-4) (2013) 239–243.
[8] Y. Kong, D. Yu, B. Zhang, W. Fang, S. Feng, Ultraviolet-emitting ZnO nanowires synthesized by a physical vapor deposition approach, Applied Physics Letters 78 (4) (2001) 407–409.
[9] R. Yousefi, F. Jamali-Sheini, A. Khorsand Zak, M. Mahmoudian, Effect of indium concentration on morphology and optical properties of In-doped ZnO nanostructures, Ceramics International 38 (8) (2012) 6295–6301.
[10] R. Yousefi, F. Jamali-Sheini, A.K. Zak, A comparative study of the properties of ZnO nano/microstructures grown using two types of thermal evaporation set-up conditions, Chemical Vapor Deposition 18 (7-9) (2012) 215–220.
[11] Y.-S. Lee, S.-N. Lee, I.-K. Park, Growth of ZnO hemispheres on silicon by a hydrothermal method, Ceramics International 39 (3) (2013) 3043–3048.
[12] R. Razali, A.K. Zak, W. Majid, M. Darroudi, Solvothermal synthesis of microsphere ZnO nanostructures in DEA media, Ceramics International 37 (8) (2011) 3657–3663.
[13] A. Khorsand Zak, W. Abd Majid, M. Mahmoudian, M. Darroudi, R. Yousefi, Starch-stabilized synthesis of ZnO nanopowders at low temperature and optical properties study, Advanced Powder Technology (2012).
[14] A.K. Zak, W. Majid, M. Darroudi, R. Yousefi, Synthesis and characterization of ZnO nanoparticles prepared in gelatin media, Materials Letters 65 (1) (2011) 70–73.
[15] A.K. Zak, M.E. Abrishami, W. Majid, R. Yousefi, S. Hosseini, Effects of annealing temperature on some structural and optical properties of ZnO nanoparticles prepared by a modified sol–gel combustion method, Ceramics International 37 (1) (2011) 393–398.
[16] A. Khorsand Zak, W. Abd Majid, H. Wang, R. Yousefi, A. Moradi Golsheikh, Z. Ren, Sonochemical synthesis of hierarchical ZnO nanostructures, Ultrasonics Sonochemistry (2012).
[17] A. Kamalianfar, S.A. Halim, Naseri Mahmoud Godarz, M. Navasery, Ud Fasih Din, J.A.M. Zahedi, Behzad Kasra, K.P. Lim, A. Lavari Monghadam, S.K. Chen, Growth and characterization of Zno multipods on functional surfaces with different sizes and shapes of Ag particles, Chinese Physics B 22 (2013) 088103.
[18] A. Kamalianfar, S.A. Halim, Jahromi Siamak Pilban, M. Navasery, Fasih Ud Din, K.P. Lim, S.K. Chen, J.A.M. Zahedi, The synthesis and characterization of peach-like Zno, Chinese Physics Letters 29 (2012) 128102.
[19] F. Jamali-Sheini, R. Yousefi, Electrochemical synthesis and surface characterization of hexagonal Cu–ZnO nano-funnel tube films, Ceramics International 39 (4) (2013) 3715–3720.
[20] T. Voss, C. Bekeny, L. Wischmeier, H. Gafsi, S. Borner, W. Schade, A. Mofor, A. Bakin, A. Waag, Influence of exciton-phonon coupling on the energy position of the near-band-edge photoluminescence of ZnO nanowires, Applied Physics Letters 89 (18) (2006) (182107-182107-182103).
[21] B. Lin, Z. Fu, Y. Jia, Green luminescent center in undoped zinc oxide films deposited on silicon substrates, Applied Physics Letters 79 (7) (2001) 943–945.
[22] N. Garces, L. Wang, L. Bai, N. Giles, L. Halliburton, G. Cantwell, Role of copper in the green luminescence from ZnO crystals, Applied Physics Letters 81 (4) (2002) 622–624.
[23] H. Zeng, W. Cai, Y. Li, J. Hu, P. Liu, Composition/structural evolution and optical properties of ZnO/Zn nanoparticles by laser ablation in liquid media, The Journal of Physical Chemistry B 109 (39) (2005) 18260–18266.
[24] K. Vanheusden, C. Seager, W.T. Warren, D. Tallant, J. Voigt, Correlation between photoluminescence and oxygen vacancies in ZnO phosphors, Applied Physics Letters 68 (1996) 403.